Available online at www.sciencedirect.com

ScienceDirect

Ceramics International 40 (2014) 1405–1414

CERAMICS INTERNATIONAL

www.elsevier.com/locate/ceramint

Life time of new SYSZ thermal barrier coatings produced by plasma spraying method under thermal shock test and high temperature treatment

Mohammad Reza Loghman-Estarki[a,*], Reza Shoja Razavi[b], Hossein Edris[a], Mousa pourbafrany[b], Hossein Jamali[b], Reza ghasemi[b]

[a]Department of Materials Engineering, Isfahan University of Technology, Isfahan, P.O. Box. 84156-83111, Islamic Republic of Iran
[b]Department of Material Engineering, Malek Ashtar University of Technology, Isfahan, Shahin-shahr, Islamic Republic of Iran

Received 10 May 2013; received in revised form 3 July 2013; accepted 4 July 2013
Available online 3 August 2013

Abstract

Nanostructured scandia (4.6 mol%), yttria (0.4 mol%) doped zirconia (5SYSZ) and 7 wt% yttria stabilized zirconia (7YSZ) thermal barrier coatings (TBCs) were produced by plasma spraying on nickel-based superalloy substrates with NiCrAlY as the bond coat. The thermal shock behavior of the two as-sprayed TBCs at 1000 °C was investigated. The results indicated that the thermal cycling lifetime of 7YSZ TBCs was longer than the 5SYSZ TBCs due to the lower thermal mismatch stress between the ceramic layer and the metallic layer at high temperature. However, the nanostructured 5SYSZ coating had higher thermal stability than 7YSZ TBC.

Keywords: C. Thermal shock resistance; Atmospheric plasma spraying; Durability of TBCs under thermal cycling; Nanostructured thermal barrier coatings

1. Introduction

Thermally sprayed thermal barrier coatings (TBCs) have been used successfully in gas turbine components to protect the metal parts from hot burner gases. This had led to further increase in operating temperature and some decrease in the amount of cooling air [1–4]. Nowadays, state-of-the-art 7 wt% yttria stabilized zirconia (7YSZ) is widely used as standard TBC top coat material [5,6]. However, the most critical issue for YSZ is the limited operation temperature (< 1.523 K) for long-term applications. At higher temperature, phase transformations and porous coating sintering result in the formation of cracks in the coating and higher thermal conductivity, and accelerate the spallation failure of TBCs [7,8]. Therefore, investigation of novel TBC materials with ultra-high temperature capability, low thermal conductivity and long-term life time is a key problem for the next generation turbine engines. Some ceramic materials such as La_2O_3–Y_2O_3–ZrO_2, Gd_2O_3–Y_2O_3–ZrO_2, $La_2Zr_2O_7$, $La_2Ce_2O_7$, $LaMgAl_{11}O_{19}$ and other kinds of rare earth doped zirconia [9–19] have been investigated as potential TBC materials. In recent years, nanostructured zirconia based TBCs deposited by atmospheric plasma spraying have been the focus of attention. It was reported that nanostructured thermal barrier coatings had high bonding strength [20], low thermal conductivity [21,22] and prolonged thermal cycling lifetime [23–27]. Accordingly, nanostructured TBCs are expected to provide better performance than the conventional TBCs.

Recently, codoping YSZ with Al_2O_3, Sc_2O_3, Y_2O_3, Bi_2O_3, Sm_2O_3, Yb_2O_3, CeO_2, etc. has attracted researchers to improve thermal and electrical properties of this ceramic [10,11]. The YSZ had the phase stability up to 1200 °C, but upon doping YSZ with scandium oxide (scandia, at specific content), the thermal stability of this ceramic was improved up to 1400 °C [10]. Increasing the thermal stability of zirconia ceramics has high potential applications in improving the efficiency and performance of engine [1,11]. Jang [14] reported that the amount of tetragonal phase was increased by codoping zirconia with scandia and yttria. This was

*Corresponding author. Tel.: +98 312 522 5041; fax: +98 312 5228530.
E-mail addresses: mr.loghman@ma.iut.ac.ir, loghman57@gmail.com (M.R. Loghman-Estarki).

0272-8842/$ - see front matter © 2013 Elsevier Ltd and Techna Group S.r.l. All rights reserved.
http://dx.doi.org/10.1016/j.ceramint.2013.07.023

due to the lower stabilization of zirconia by scandia [10,14]. The strength of the codoped material was almost 10% higher than that of the reference material (YSZ and ScSZ) [10]. It was also reported that a higher fracture toughness of the codoped material was obtained, as compared to the reference material, in accordance with the higher tetragonal phase content and the resulting enhanced transformation toughening [10,14].

So far, there has been no report on the thermal shock resistance of tetragonal scandia, yttria codoped zirconia (t-SYSZ) TBC. It is necessary to investigate thermal shock behavior of SYSZ coating and the related failure mechanism of it in order to seek the possibility of using SYSZ as TBC materials. In this work, 5SYSZ TBCs were sprayed onto Ni-based superalloy by atmospheric plasma spraying. Then, thermal shock behavior of this coating was compared to t-7YSZ APS coating.

2. Experimental section

2.1. Materials and procedures

Thermal barrier coatings, composed of a bond coating and a top coating, were air-plasma-sprayed on a Ni-based superalloy (Inconel 738, Ni–15Cr–8.5Co) substrate. The substrate geometry was a square of $10 \times 10\ mm^2$ surface area with 10 mm thickness. The spraying material for the bond coat was commercial $Ni_{22}Cr_{10}Al_1Y$ (wt%, Metco 204NS powder, particle size of 11–125 μm) and the top coat was nanostructured scandia–yttria stabilized zirconia (SYSZ, ZrO_2–0.6 mol% Y_2O_3 4.6 mol% Sc_2O_3) and yttria stabilized zirconia (ZrO_2–7 wt% Y_2O_3). The ceramic powders of nanostructured 7YSZ (Nanox S4007 powder consisting of agglomerated nanosized particles 15–150 μm in diameter) were purchased from Inframat Company. The SYSZ nanogranules were fabricated in the laboratory from their nanopowders. Because of the poor flow ability of the original nanostructured SYSZ that made it unsuitable for plasma spraying, the SYSZ nanopowders were agglomerated by the spray drying [2,10] method. First, a water-soluble binder of 5 wt% (in accordance to content of SYSZ nanopowders in suspension) polyvinyl alcohol (PVA) in mass fraction in water at 95 °C was prepared. After cooling to room temperature, an organic binder of PVA was prepared. Then, the nanostructured SYSZ and the organic blinder of PVA were evenly mixed by a stirrer. After that, the mixtures were spray dried using laboratory spray drying apparatus. The main controlled operating parameters were the air temperature at the entry (220–235 °C), at the exit (135–140 °C), inside the chamber (180 °C), the rotate speed of atomizer (17,000 rpm), and the air (4.4–4.6 l/h) and slurry flow rates (1–1.2 kg/h). Finally, semi-spherical and irregular SYSZ agglomerated nanoparticles were obtained. The reason for the obtained morphology by the spray drying method was discussed in our recent research [2]. The particles size in the range of 20–150 μm was chosen for plasma spraying by passing them through a sieve (100 and 500 US mesh). Some specifications of powders are shown in Table 1. Prior to spraying process, the substrates were successively ground with SiC paper up to 800# (10 μm). They were then cleaned by absolute ethyl alcohol in an ultrasonic set. The as-sprayed substrates were then grit blasted by alumina particles with the size of 125 μm. Subsequently, the substrates were placed into the air plasma spray (APS) system (Switzerland PT Corporation, Plasma-Technik A3000S) for overlaying with NiCrAlY bond coating. Nanostructured YSZ and SYSZ were sprayed onto as-sprayed bond coat specimen by an APS system. The APS parameters for depositing bond coat and top coat are given in Ref. 2,4.

2.2. Thermal shock test

The thermal shock test was carried out in a muffle furnace. When the temperature of the furnace reached up to 1000 °C, the specimens were pushed into the furnace. The specimens were held for about 10 min in the furnace, and then they were directly quenched into water. As the water for test was so capacious, the temperature rise of water was not obvious. After 60 s, the temperature of specimens was the same as water according to the test of a thermometer contacting the surface of specimens. The temperature of water throughout the cycling was between 23 and 27 °C. When the samples were cooled to the ambient temperature, they were taken out, dried and put into the high temperature furnace again, repeating the same process. More than 20% of the cracked and spalled regions of the surface of top coating were adapted as the criterion for the failure of the coating. The macroscopic images of the samples in time during the thermal shock test were captured using a digital camera. The weight changes of the samples were measured to a precision of 0.1 mg by an analytical balance (TE214S, Sartorius, Germany). The water-quenched thermal shock test was also performed by other investigations [4,18].

2.3. Coating characterization

The microstructure of as-sprayed coatings was investigated by a field emissions scanning electron microscope (FESEM; S-4160, Hitachi Ltd., Japan). The phase analysis was carried out by the X-ray diffractometry (XRD; BrukerD8 Advance diffractometer, Germany) with filtered Cu-Ka radiation (0.15406 nm). In order to cater for microstructural and elemental analyses of samples after thermal shock test, scanning electron microscope (Seron Technology-AIS-2000, Korea) equipped with an energy dispersive spectrometer (EDS) was used. The surface roughness (Ra) of substrates prior to spraying was measured by a roughness tester (MitutoyoSJ-201P, Japan). The measured surface roughness (Ra) of substrates was 9.10 μm. The nanoindenter NHTX S/N 01-03119 with a Berkovitch-type diamond tip was used to determine the elastic modulus (E) of ceramic coatings. Indenting was done on well-polished cross-section. The load used was 10 mN (20 mN loading and unloading rate) and the dwell time was 17 s. At least, six indentations on the polished cross section were performed and averaged. The percentage of nano-zones (non-melted area) was estimated by image analysis software from SEM image of polished cross section of samples.

Table 1
Some specifications of powders used for plasma spraying.

Type of material	Particle size before and after agglomeration	Morphology	Manufactured method, purchase
7YSZ	60–80 nm, 20–95 μm	Spherical	Inframat company
5SYSZ	40–50 nm, 20–130 μm	Irregular	Sol–gel, spray drying and calcination
NiCrAlY	45–90 μm	Spherical	Sulzer metco, gas atomized

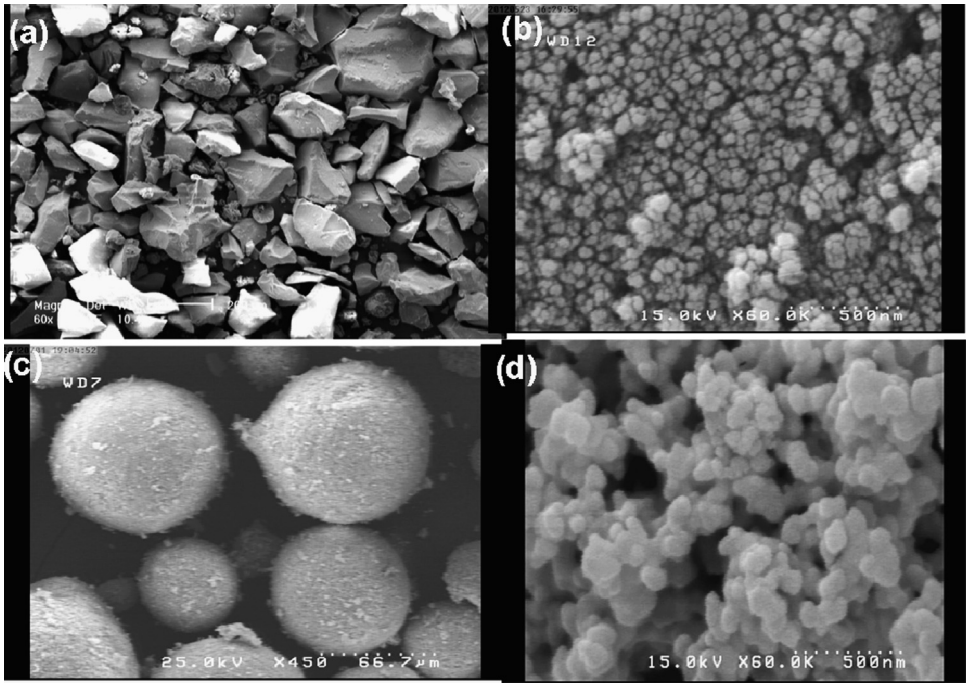

Fig. 1. Surface morphology of thermal sprayed feedstock: (a,b) nanostructured 5SYSZ (c,d) nanostructured 7YSZ feedstock.

3. Results and discussion

3.1. Microstructure of the feedstock and its corresponding coating

Fig. 1 shows the morphology of the two kinds of feedstocks. From Fig. 1(a), it is clear that the SYSZ feedstock exhibits polyhedral, irregular and angular shape with different sizes ranging from 20 μm to 130 μm. This may due to obtaining it from sol–gel in the actual process. This affects its flowability and decreases the deposition efficiency more or less in the plasma spraying process. The nanostructured YSZ feedstock (Fig. 1c) was composed of spherical/equiaxed shape of nanostructured agglomerates with the size of 20–95 μm (Table 1). It can be designated as sphere package structure. From high magnification image of each granule (Fig. 1b,d), it is clearly observed that their microstructures were composed of nanoparticles with diameter of nearly 40–60 nm.

Fig. 2 displays the XRD patterns of the two feedstocks and their corresponding coatings. The nanostructured 7YSZ feedstock was mainly composed of t phase (Fig. 2a). The corresponding coating was predicted to be composed of t′ phase after plasma spraying process (Fig. 2b). This tetragonal zirconia phase, which was observed in as-sprayed coating, was mainly composed of so called non-transformable phase t′. It had lower c and c/a when compared with the t phase (where a, c denotes the lattice parameters) [4,20]. The free yttria (or scandia) phase was not observed in the XRD pattern of the nanostructured as-sprayed zirconia coatings. It is usually recognized that the t′ phase resulted from the high temperature cubic phase by diffusion less transformation at high quenching rate of 10^6 K/s. The t phase was normal tetragonal phase and the content of the Y_2O_3 in the t phase was lower when compared with t□ phase. The SYSZ nano-agglomerated feedstock formed non- transformable tetragonal phase in the process of spray drying granulation, and the t□-phase was kept stable during the plasma spraying, indicating that the phase structure of SYSZ coating was very stable (Fig. 2e,f).

Fig. 3 presents the polished cross sections of as-sprayed nanostructured TBCs, which are composed of the YSZ or SYSZ top coat and NiCrAlY bond coat deposited on the superalloy substrate by APS process. According to this figure, both top coatings are well bonded to the bond coating. The fractured cross section morphologies of both nanostructured coatings are shown in Fig. 4. It should be noted that two types of microstructure are present in both nanostructured coatings (Fig. 4): The columnar

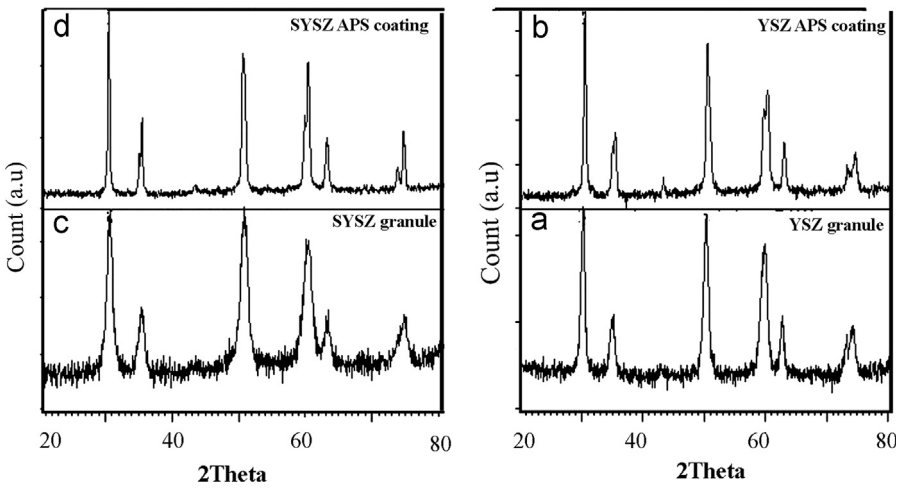

Fig. 2. XRD patterns of thermal sprayed feedstocks and their corresponding coatings (a,b) nanostructured 7YSZ, and (c, d) nanostructured 5SYSZ.

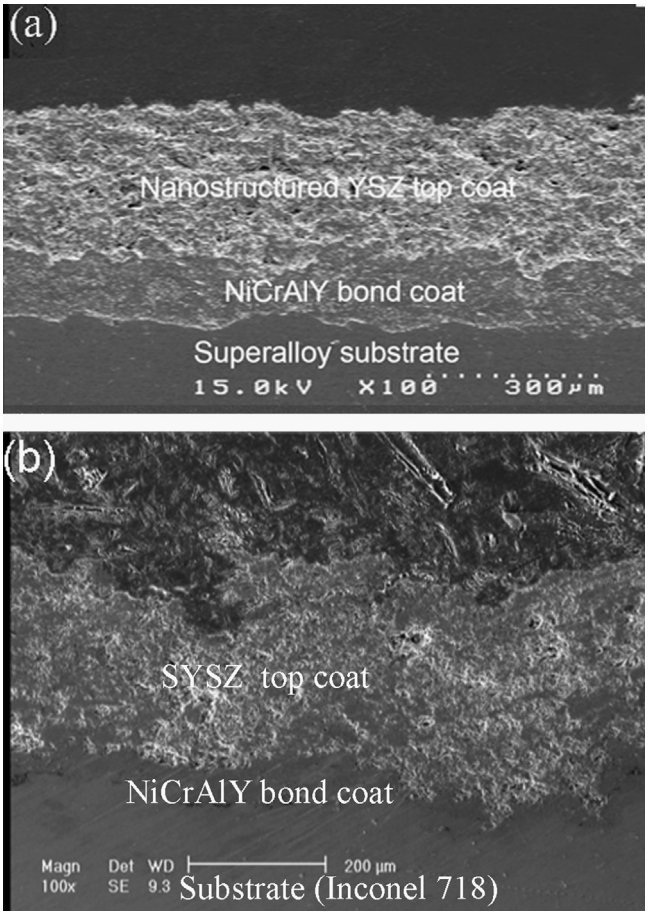

Fig. 3. FESEM micrographs of polished cross section of as-sprayed TBC with nanostructured (a) 7YSZ and (b) 5SYSZ.

grains were solidified from the melted fraction of YSZ (or SYSZ) powder and the loose microstructure was retained from the unmelted YSZ (or SYSZ) powder [2,4,20]. Therefore, both coatings exhibited a bimodal microstructure consisting of nanosized particles retained from the powder and microcolumnar grains formed through the solidification of the melted fraction in spray particles. The percentage of nano-zones embedded in the 7YSZ coating structure was approximately $26 \pm 2\%$. The SYSZ coating showed the lower percentage of partially melted area (nanozone, $20 \pm 3\%$) due to its different melting degree of irregular feedstock in comparison with spherical ones [2,20]. The nano-zones contained a large volume fraction of pores with size ranging from several tens to several hundreds of nanometers. This porous structure could enhance the thermal insulation effect of TBCs [16–20].

3.2. Thermal shock behaviors of TBCs

Fig. 5 shows the macroscopic images of the nanostructured TBCs during thermal shock testing. When the "edge effect" was considered in terms of the practical application of thermal barrier coatings, such as edges and corners in combustor and blade rim, square specimens were used. As can be seen, for both coatings, starting failure from the edges of the sample was occurred and then propagated to the adjacent areas. Beginning of the failure from the edges was due to the extreme heating and cooling conditions encountered and singularity of thermal stresses at the edges. Other studies [4,26,27] have also mentioned the edge effect on failure during thermal cycling.

Fig. 6 presents weight changes as a function of cycle number for both kinds of nanostructured samples during thermal shock testing. Based on this figure, the nanostructured 7YSZ coating exhibited a better performance than 5SYSZ one during thermal shock testing. As can be seen, the weight of both samples was first increased due to substrate free surface oxidation and then reduced suddenly after some cycles. After sudden weight loss, a weight gain was observed that could be due to the substrate and bond coat oxidation. Since gradual weight loss was not observed, coatings delaminations did not occur. On the other hand, the sudden weight loss of samples implied that coatings spallation could occur.

The polished cross sections of the nanostructured 7YSZ and 5SYSZ TBCs after thermal shock testing are shown in Fig. 7.

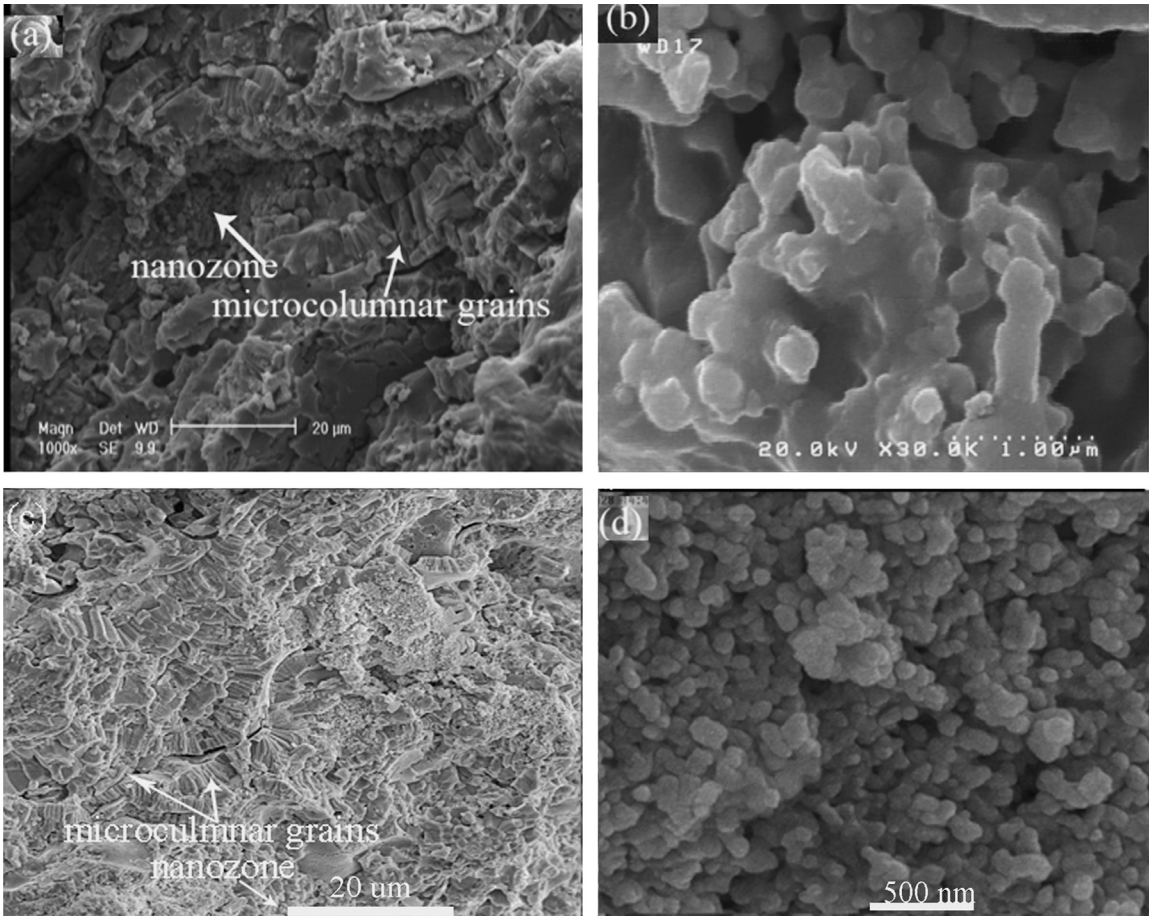

Fig. 4. FESEM micrograph of the fractured cross section of as-sprayed nanostructured (a,b) 7YSZ and (c,d) 5SYSZ.

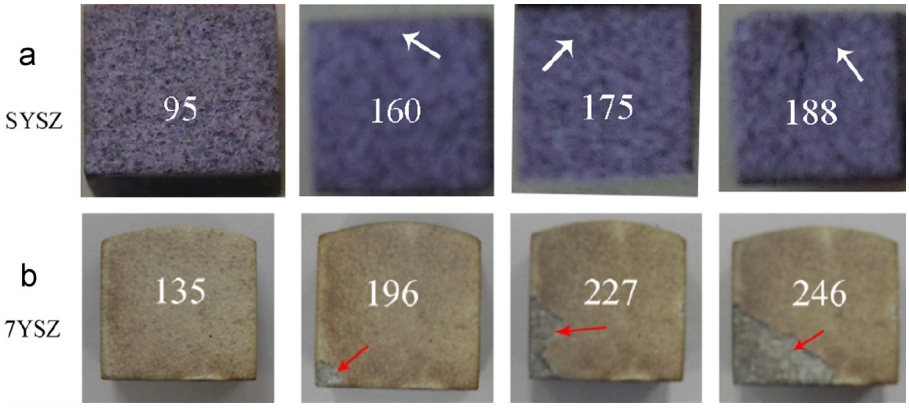

Fig. 5. Photographs of nanostructured (a) 5SYSZ (b) 7YSZ samples during thermal shock testing.

As can be seen, in both coatings, cracks were initiated within the ceramic top coat near the top coat/bond coat interface. Based on this figure, the lack of thickness loss of both coatings during thermal shock also rejected the coating delamination mechanism. Therefore, analysis of weight changes graphs (Fig. 6) and microscopic images (Fig. 7) showed that the failure of both nanostructured coatings was in a similar mode, occurring as spallation of the top coat, near and parallel to the top coat/bond coat interface. Research shows that after thermal shock tests, four types of cracks were formed in the TBCs, i.e., vertical crack, horizontal crack, propagating crack, and penetrating crack [23]. In penetrating crack, vertical cracks penetrate the bond coat to the substrate surface. In the current work, after thermal cycles, vertical cracks and propagating crack (or horizontal crack) emerged in the SYSZ and YSZ top coat (Fig. 7). However, the penetrating crack and no obvious oxide were generated at the bond coat and the substrate interface, which was different from Li work [23] on thermal failure of nanostructured TBCs.

The previous studies [27–29] showed that oxidation of the bond coat and thermal mismatch stress were the main factors

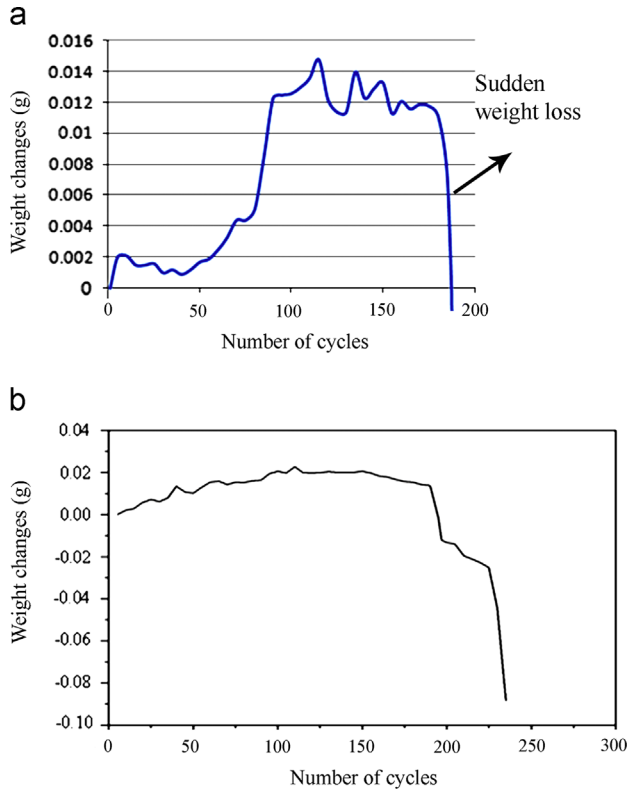

Fig. 6. Weight changes as a function of cycle number for (a) SYSZ (b) 7YSZ TBCs during thermal shock testing.

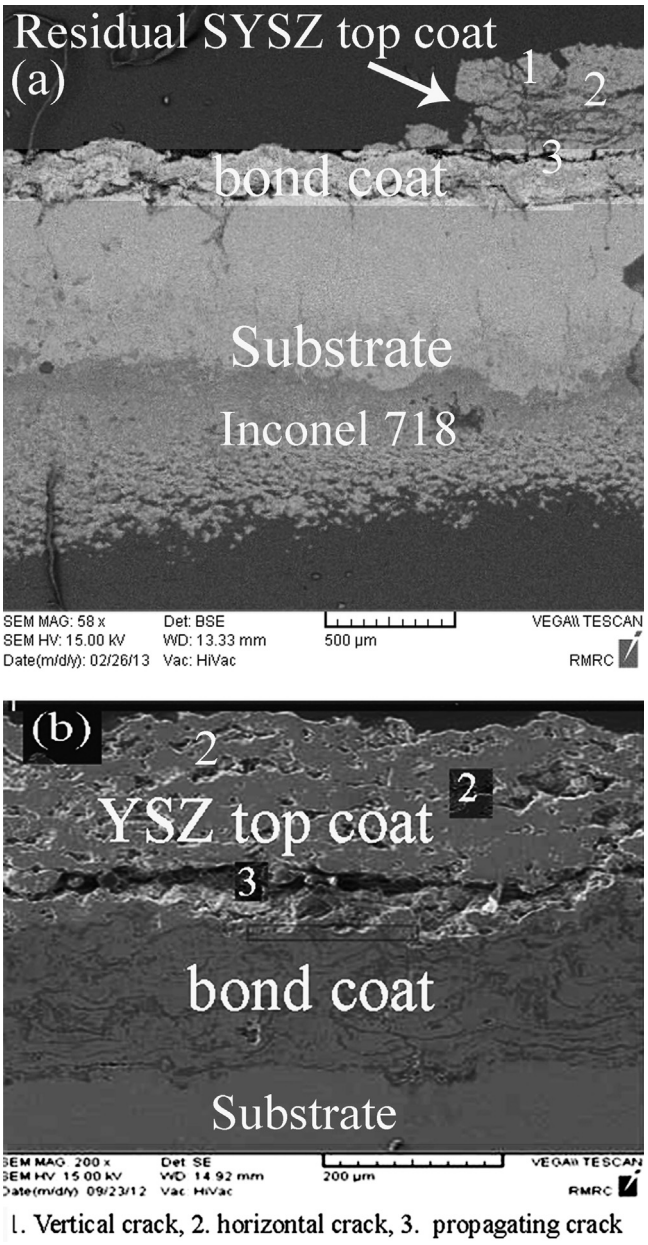

Fig. 7. SEM micrographs of polished cross section of nanostructured (a) SYSZ with thickness of 250 ± 20 µm, (b) 7YSZ TBCs after 188 and 246 cycles, respectively.

influencing degradation of TBCs. The EDS analyses of top coat/bond coat interfaces of both nanostructured TBCs after thermal shock testing are shown in Fig. 8. Based on these analyses, for both coatings, thermally grown oxide (TGO) was not formed on the top coat/bond coat interface. The SEM micrographs of samples after thermal shock testing (Fig. 7) also confirm the lack of formation of TGO. Therefore, it can be concluded that bond coat oxidation did not occur during thermal cycling, thereby not contributing to the coating failure. It seems that the lack of visible thickness formation of TGO is due to short heating time [29,30].

Fig. 9 presents the XRD patterns of nanostructured TBCs coatings after failure. According to XRD patterns (Fig. 9a,b), as-sprayed 5SYSZ and 7YSZ coatings were completely made of a non-transformable tetragonal (t′) phase. After long-term thermal cycling, the metastable non-transformable tetragonal phase may be decomposed into low stabilizer tetragonal phase by the diffusion of the stabilizer (Y_2O_3 or Sc_2O_3), and the low stabilizer tetragonal phase may be transformed to the monoclinic phase. The tetragonal-to-monoclinic phase transformation is martensitic in nature and it is accompanied by a significant volume increase of approximately 3–5 vol%, affecting the integrity of the coating [4,28–30]. Anyway, in this study, no phase change was observed during the thermal shock of 5SYSZ and 7YSZ coatings. Accordingly, stresses resulting from phase transformation had no contribution to degradation of both coatings. In layered systems, the coefficient of thermal expansion is an important property because the thermal stress resulting from the coefficient of thermal expansion (CTE, α) mismatch between the layers may lead to degradation. Therefore, CTE mismatch can be one of the key factors responsible for the failure of TBCs.

The substrate and bond coat, due to the relatively same chemical compositions, have low CTE mismatch. But, since the difference in CTE between the ceramic top coat and the underlying metallic components is high, it can be anticipated that top coat/bond coat interface stresses are more upon heating/cooling of the substrate/coating system. Therefore, thermal stresses caused by the mismatch of the thermal expansion are concentrated on the interface between ceramic

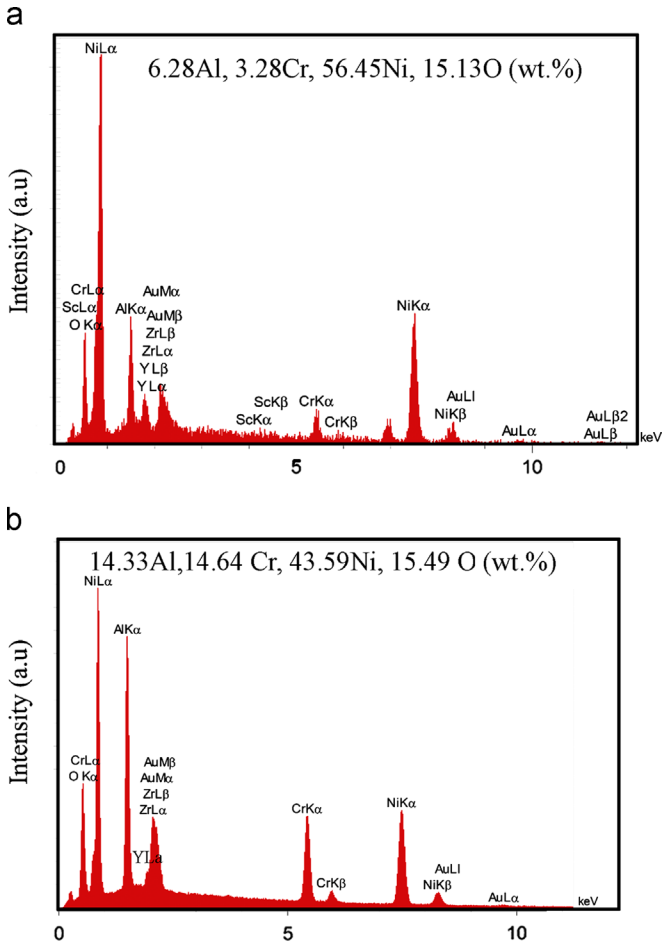

Fig. 8. EDS analyses from top coat/bond coat interface of nanostructured (a) SYSZ (b) 7YSZ TBCs after failure.

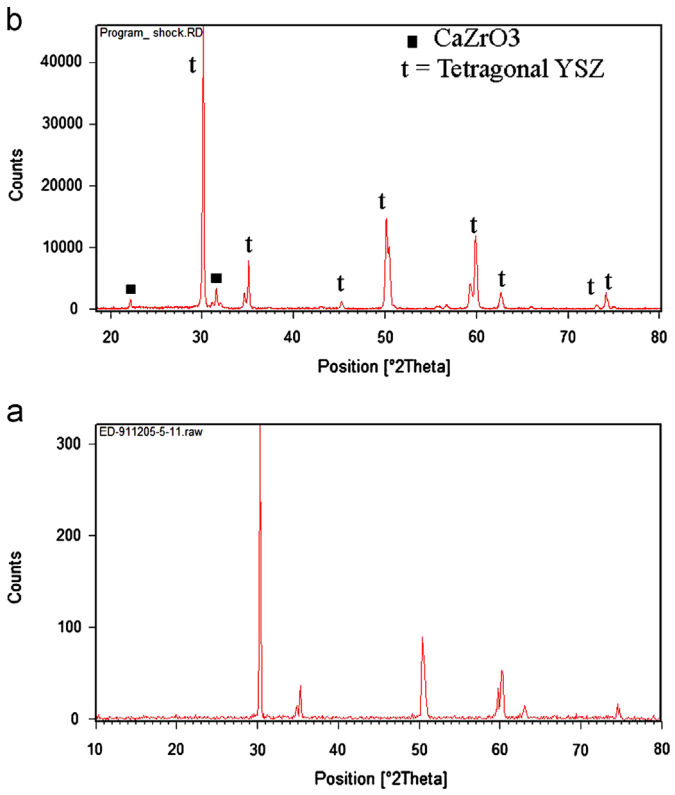

Fig. 9. XRD patterns of nanostructured (a) SYSZ (b) 7YSZ coatings after thermal shock testing.

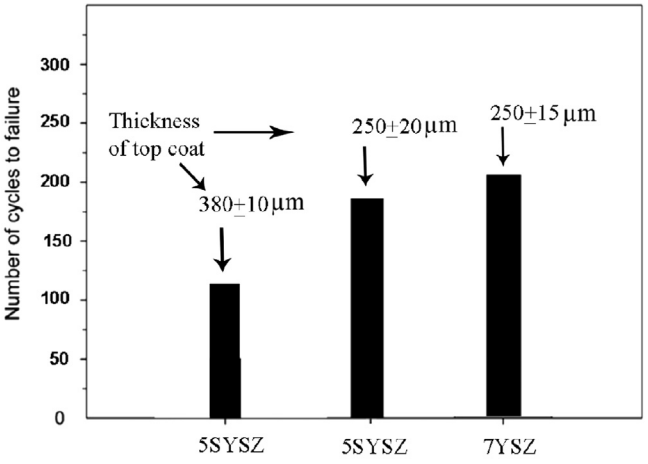

Fig. 10. The thermal cycling life times of the nanostructured TBCs.

top coat and metallic bond coat. With continuous exposure of samples to thermal cycles, these stresses result in crack nucleation and propagation in the ceramic top coat. Later, these initial cracks assist each other and with propagation in the top coat, near and parallel to top coat/bond coat interface, finally result in top coat spallation. Therefore, during thermal shock testing, the failures of both nanostructured 5SYSZ and 7YSZ coatings were dominated by thermal stresses generated due to the difference in CTE between the ceramic top coat and the underlying metallic components. The crack formation and propagation in the top coat and the remaining little parts of top coat on the bond coat (Fig. 7) also confirm this fact.

3.3. Thermal shock lifetime

Thermal shock resistance depends on the size and distribution of pores or existing cracks in the coating. Thermal cycling can result in the cracking and spalling of TBC. It is due to the fact that cyclic thermal loads can cause horizontal or vertical cracks to propagate, resulting in delamination/spallation of the coating and loss of thermal protection to the substrate. The thermal cycling life times of both nanostructured TBCs are graphically presented in Fig. 10. It can be seen that the nanostructured 7YSZ TBC exhibits an excellent average thermal cycling lifetime, approximately 1.13 times higher than the 5SYSZ TBC (average thermal shock lifetime of SYSZ for two sample was (188+247) no. of cycle/2 = 217 cycle).

When the coating specimen was taken out from the high temperature furnace and quickly quenched in water in the process of thermal cycling, a very large stress was developed in the coating due to the difference of thermal expansion coefficients between the ceramic layer and the metallic

substrate, which can be given by the following expression:

$$\sigma_c = \Delta\alpha\Delta T E/(1-\nu^2) \quad (1)$$

where σ_c is the developed stress in the coating, and E and ν are Young's modulus and Poisson ratio of the ceramic coating, respectively. $\Delta\alpha$ is the difference in CTE between the ceramic coating and the metallic substrate, and ΔT is the change in temperatures. The α coefficient of Inconel 738 Ni-based substrate, plasma-sprayed NiCrAlY bond coat, and plasma-sprayed top coat at 1000 °C is reported to be $17.5\times10^{-6}\,°C^{-1}$ [3], $15\times10^{-6}\,°C^{-1}$ [3] and $11.7\times10^{-6}\,°C^{-1}$ (7YSZ), $11.5\times10^{-6}\,°C^{-1}$ (SYSZ), [3,23], respectively. By keeping Poisson ratio and elastic modulus value equal to 0.12 and 26 GPa [23], the thermal expansion mismatch stress value (σ_c) of 7YSZ and 5SYSZ was obtained to be −0.142 GPa and −0.147 GPa, respectively. This result shows that 5SYSZ sustains more CTE stress than 7YSZ TBCs. Furthermore, the elastic modulus of 7YSZ (median of six nanoindentation = 161.49 Gpa) coating, as compared to the 5SYSZ (185.98 Gpa) coating, was lower. This caused an increase in the compliance capabilities and thermal relaxation of its coating as compared to its 5SYSZ counterpart. Since the CTE of the metallic substrate and bond coat, as compared to the ceramic top coat, is very high, a larger CTE of the top coat means a lower thermal mismatch between the top coat and bond coat layers. Thus, it can be expected that the main factor in TBC failure, i.e., the thermal stress generated during the thermal cycling, is lower for nanostructured tetragonal 7YSZ coating, as compared to the 5SYSZ one.

Comparison of weight change curves (Fig. 6) shows that the failure (a destruction of more than 20% in the coating surface) of nanostructured 7YSZ TBC, as compared to the 5SYSZ TBC, has occurred in more stages. Based on 7YSZ coating, a smaller surface of the coating is degraded in each stage than in the 5SYSZ coating.

The thickness of the coating also has a very strong impact on the thermal shock life time of the as-sprayed coating. Fig. 11 shows the polished cross sections of the nanostructured 5SYSZ TBCs, with thickness of 380 μm, after thermal shock testing. As can be seen, the failure of these coatings was in a mode similar to 7YSZ and 5SYSZ (thickness of 220–240 μm), occurring as the spallation of top coat, near and parallel to the top coat/bond coat interface. Furthermore, penetrating crack and obvious oxide were generated at the bond coat and the

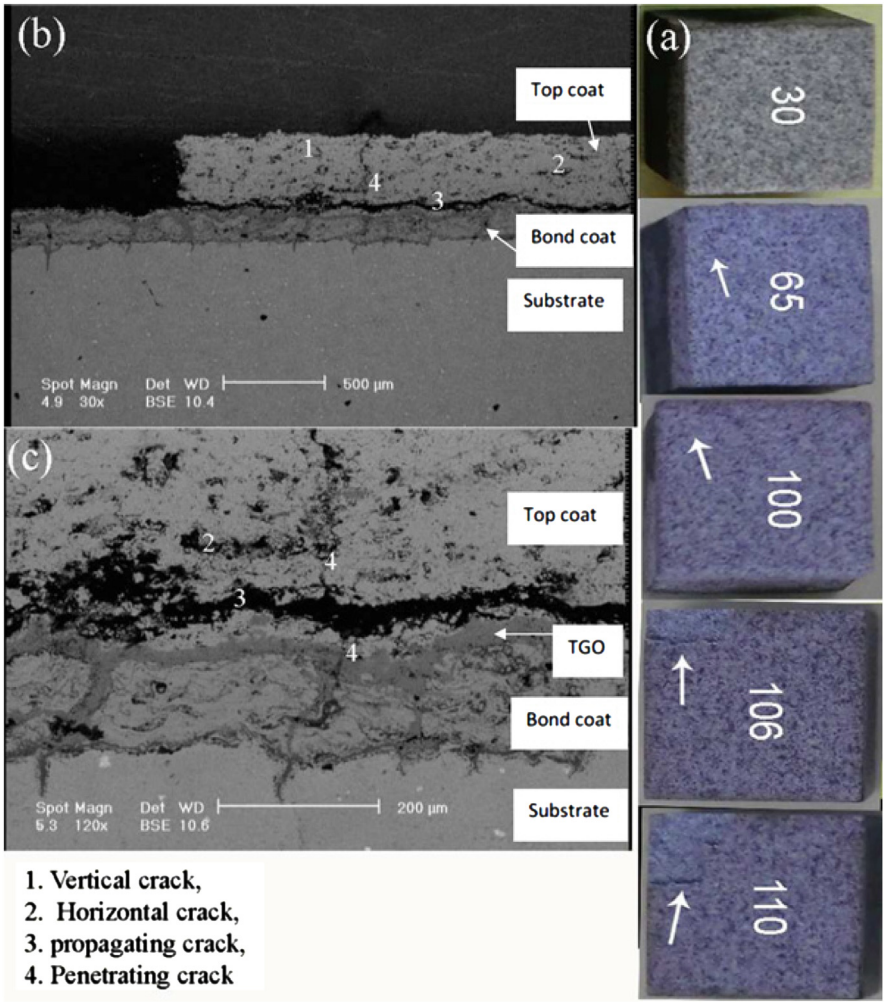

Fig. 11. (a) Photographs of nanostructured (b,c) SEM images (with different magnification) of polished cross section of nanostructured SYSZ, with thickness of 380 μm for top coat, after 110 cycle of thermal shock testing.

substrate interface, different from thermal failure of nanostructured 7YSZ and 5SYSZ (thickness = 220–240 μm) TBCs. It was explained that TBCs thicker than 300 μm are susceptible to cracking and delamination occurs either during spraying or upon thermal cycling [18].

Indeed, the thick TBC will be beneficial to the improvement of the thermal insulation effect, but the higher stress will be produced in the thick TBC which makes the thermal cycling lifetime decline when it is exposed to high temperature environment. When the thickness of the coating is high, it can bring about the following effects: first, greater thermal gradient will be caused in the thick TBC during the thermal shock across the whole coating thickness and consequently, higher thermal stresses will be produced within the whole coating system. Second, both the elastic strain energy stored and the energy release rate for a crack will also be increased. These two factors will promote the failure of the thick coatings. Anyway, in the current work, more vertical cracks (and penetrating cracks) were produced when the thickness of the SYSZ nanocoating was increased from 230 ± 10 μm to 380 ± 15 μm. It was due to the higher tensile stress in plane [6,18]. So, the amount of oxygen migrated by diffusion through the top coat was increased. So we can expect a higher TGO growth (EDX result: before thermal shock in bond coat we have 5–10 wt% Al, after thermal shock there is 27 wt% Al and 14.2 wt% O in local TGO in bond coat of Fig. 11) rate and as a result, a lower thermal shock resistance.

3.4. High temperature stability of TBCs at 1400 °C/24 h

Increasing thermal stability of zirconia based ceramic could have a high potential application in the improvement of gas turbine rendement [2,6]. In order to investigate thermal stability of SYSZ and YSZ TBCs, the free-standing coatings were put into the furnace, maintained at temperature of 1400 °C for 24 h, and cooled to room temperature. The XRD patterns of both coatings and heat treatment at this temperature are shown in Fig. 12. As can be seen, there was no monoclinic phase in 5SYSZ coating (Fig. 12a). But, in the case of 7YSZ coating, the main peaks of monoclinic phases (m($\bar{1}$11) and m (111)) appeared (Fig. 12b,c). The volume fractions of m-ZrO_2 (%m), as the criterion for coatings destabilization during high temperature treatment, are compared in Table 2 and calculated by the peak intensity ratio formula [4,26]:

$$\%\mathrm{m} = \frac{I_m(1^-11) + I_m(111)}{I_m(1^-11) + I_m(111) + I_t(111)} \times 100 \quad (2)$$

where I represents the diffraction intensity of the respective lattice planes. According to Eq. (2), the nanostructured SYSZ coating has a higher thermal stability than that of the 7YSZ TBC, which can be attributed to its higher amount of tetragonal phase [10,14].

4. Conclusions

The flawless performance of TBCs is a very important subject in the industry. Since contribution of these coatings in turbine engine efficiency is undeniable, their durability against high temperature thermal cycles is very important. Therefore, the thermal shock resistance of plasma-sprayed nanostructured 5SYSZ and 7YSZ TBCs was investigated in a comparative aspect. The major conclusions are as follows:

(1) In all cases, the initial cracks were generated at the corner of the square specimen.
(2) The failures of both nanostructured TBCs were due to the spallation of top coat, near and parallel to top coat/ bond

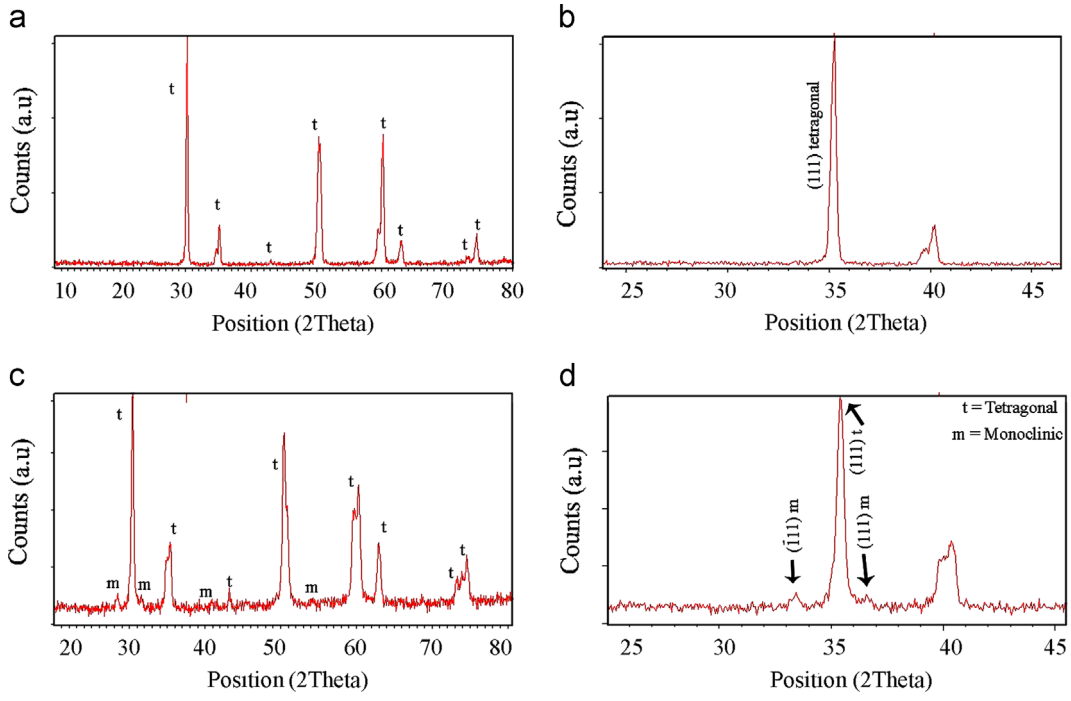

Fig. 12. The XRD patterns of the (a,b) SYSZ (c,d) 7YSZ coatings after heat treatment at temperature of 1400 °C for 24 h.

Table 2
The volume fractions of m-ZrO_2 (%m) during high temperature thermal treatment (1400 °C/24 h).

Type of material	7YSZ	5SYSZ
(%m)	> 2	0

coat interface. The thermal stress caused by the difference in CTE between the ceramic top coat and the underlying metallic components was identified as the major factor of TBC failure.

(3) The nanostructured SYSZ TBC exhibited improved thermal stability (no destabilization) at 1400 °C as compared to the 7YSZ TBC. It can be attributed to the higher amount of tetragonal phase of the nanostructured SYSZ coating.

Acknowledgments

The authors wish to acknowledge Malek-Ashtar University of Technology for support for this study. The authors would also like to thank M. Hajizadeh-Oghaz, Mr. Mahmoudi and Dr. Zia Valefi for their cooperation.

References

[1] M. Hajizadeh Oghaz, R. Shoja Razavi, M.R. Loghman-Estarki, R. Ghasemi, Optimization of morphology and particle size of modified sol–gel synthesized YSZ nano powder using Taguchi method, Journal of Nano Research 21 (2013) 65.
[2] M.R. Loghman-Estarki, R. Shoja Razavi, H. Edris, R. Ghasemi, Spray drying of nanometric SYSZ powders to obtain plasma sprayable nanostructured granules, Ceramic International (2013) (in press).
[3] C.R.C. Lima, J.M. Guilemany, Adhesion improvements of thermal barrier coatings with HVOF thermally sprayed bond coats, Surface and Coatings Technology 201 (2007) 4694–4701.
[4] H. Jamali, R. Mozafarinia, R. Shoja Razavi, R. Ahmadi-Pidani, Fabrication and evaluation of plasma-sprayed nanostructured and conventional YSZ thermal barrier coatings, Ceramics International 38 (2012) 6712–6805.
[5] Z. Hong, L. Fei, H. Bo, W. Jun, S. Bao-de, Nanostructured yttria stabilized zirconia coatings deposited by air plasma spraying, Transactions of Nonferrous Metals Society of China 17 (2007) 389–393.
[6] L. Wang, Y. Wang, X.G. Sun, J.Q. He, Z.Y. Pan, C.H. Wang, Thermal shock behavior of 8YSZ and double-ceramic-layer $La_2Zr_2O_{7/8}$YSZ thermal barrier coatings fabricated by atmospheric plasma spraying, Ceramics International 38 (2012) 3595–3606.
[7] P. Fauchais, G. Montavon, R.S. Lima, B.R. Marple, Engineering a new class of thermal spray nano-based microstructures from agglomerated nanostructured particles, suspensions and solutions: an invited review, Journal of Physics D:Applied Physics 44 (2011) 093001.
[8] F. Davar, A. Hassankhani, M.R. Loghman-Estarki, Controllable synthesis of metastable tetragonal zirconia nanocrystals using citric acid assisted sol–gel method, Ceramics International 39 (2013) 2933.
[9] M. Matsumoto, N. Yamaguchi, H. Matsubara, Low thermal conductivity and high temperature stability of ZrO_2–Y_2O_3–La_2O_3 coatings produced by electron beam PVD, Scripta Materialia 50 (2004) 867–871.
[10] M.R. Loghman-Estarki, R. ShojaRazavi, H. Edris, Synthesis of SYSZ nanocrystal via new wet chemical method, Current Nanoscience 8 (2012) 767.
[11] R. Vassen, X. Cao, F. Tietz, et al., Zirconates as new materials for thermal barrier coatings, Journal of the American Ceramic Society 83 (2000) 2023–2028.
[12] X.Q. Cao, R. Vassen, W. Fischer, et al., Lanthanum–cerium oxide as a thermal barrier-coating material for high-temperature applications, Advanced Materials 34 (2003) 1438–1442.
[13] C. Friedrich, R. Gadow, T. Schirmer, Lanthanum hexaluminate—a new material for atmospheric plasma spraying of advanced thermal barrier coatings, Journal of Thermal Spray Technology 10 (2001) 592–598.
[14] J. Jang, K. Dae-Joon, D.Y. Lee, Unusual calcination temperature dependent tetragonalal monoclinic transitions in rare earth-doped zirconia nanocrystals, Journal of Materials Science 36 (2001) 5391.
[15] H.B. Guo, H.J. Zhang, G.H. Ma, et al., Thermo-physical and thermal cycling properties of plasma-sprayed $BaLa_2Ti_3O_{10}$ coating as potential thermal barrier materials, Surface and Coatings Technology 204 (2009) 691–696.
[16] M.R. Loghman-Estarki, R. Shoja Razavi, H. Edris, Synthesis and thermal stability of ZrO_2, Re–Sc, Y nanocrystals, Defect and Diffusion Forum 334 (2013) 60–64.
[17] X.Y. Xie, H.B. Guo, S.K. Gong, Mechanical properties of $LaTi_2Al_9O_{19}$ and thermal cycling behaviors of plasma sprayed $LaTi_2Al_9O_{19}$/YSZ thermal barrier coatings, Journal of Thermal Spray Technology 19 (2010) 1179–1185.
[18] M.R. Loghman-Estarki, et al., Comparative studies on synthesis of nanocrystalline Sc_2O_3–Y_2O_3 doped zirconia (SYDZ) and YSZ solid solution via modified and classic Pechini method, Crystal Engineering Communication 15 (2013) 5898–5904.
[19] R.J. Bratton, S.K. Lau, S.Y. Lee, Evaluation of presented-day thermal barrier coatings for industrial/utility utility applications, Thin Solid Films 73 (1980) 429–437.
[20] H. Jamali, R. Mozafarinia, R. Shoja Razavi, R. Ahmadi-Pidani, M. R. Loghman-Estarki, Fabrication and evaluation of plasma-sprayed nanostructured and conventional YSZ thermal barrier coatings, Current Nanoscience 8 (2012) 402.
[21] R.S. Lima, B.R. Marple, Toward highly sintering-resistant nanostructured ZrO_2–7 wt%Y_2O_3 coatings for TBC applications by employing differential sintering, Journal of Thermal Spray Technology 17 (2008) 846–852.
[22] R.S. Lima, A. Kucuk, C.C. Berndt, Integrity of nanostructured partially stabilized zirconia after plasma spray processing, Materials Science and Engineering A 313 (2001) 75–82.
[23] C. Zhou, Q. Zhang, Y. Li, Thermal shock behavior of nanostructured and microstructured thermal barrier coatings on a Fe-based alloy, Surface and Coatings Technology 217 (2013) 70–75.
[24] S.R. Choi, D. Zhu, R.A. Miller, Mechanical properties/database of plasma-sprayed ZrO_2–8 wt% Y_2O_3 thermal barrier coatings, International Journal of Applied Ceramic Technology 1 (4) (2004) 330–342.
[25] C. Ramachandra, K.N. Lee, S.N. Tewari, Durability of TBCs with a surface environmental barrier layer under thermal cycling in air and in molten salt, Surface and Coatings Technology 172 (2003) 150–157.
[26] R. Ahmadi-Pidani, R. Shoja-Razavi, R. Mozafarinia, H. Jamali, Improving the thermal shock resistance of plasma sprayed CYSZ thermal barrier coatings by laser surface modification, Optics and Lasers in Engineering 50 (2012) 780–786.
[27] C. Giolli, A. Scrivani, G. Rizzi, F. Borgioli, G. Bolelli, L. Lusvarghi, Failure mechanism for thermal fatigue of thermal barrier coating systems, Journal of Thermal Spray Technology 18 (2009) 223–230.
[28] A.N. Khan, J. Lu, Thermal cyclic behavior of air plasma sprayed thermal barrier coatings sprayed on stainless steel substrates, Surface and Coatings Technology 201 (2007) 4653–4658.
[29] Y. Liu, C. Persson, J. Wigren, Experimental and numerical life prediction of thermally cycled thermal barrier coatings, Journal of Thermal Spray Technology 13 (2004) 415–424.
[30] S. Ahmaniemi, P. Vuoristo, T. Mantyla, C. Gualco, A. Bonadei, R. D. Maggio, Thermal cycling resistance of modified thick thermal barrier coatings, Surface and Coatings Technology 190 (2005) 378–387.